Original Article

Institution of MECHANICAL ENGINEERS

Journal of MECHANICAL ENGINEERING SCIENCE

Proc IMechE Part C:
J Mechanical Engineering Science
2017, Vol. 231(22) 4126–4138

DOI: 10.1177/0954406216662087
journals.sagepub.com/home/pic

SAGE

Asymptotic trends in time-varying oscillatory period for a dual-staged torsional system

Michael D Krak and Rajendra Singh

Abstract

The primary goal of this article is to propose a new analysis tool that estimates the asymptotic trends in the time-varying oscillatory period of a non-linear mechanical system. The scope is limited to the step-response of a torsional oscillator containing a dry friction element and dual-staged spring. Prior work on the stochastic linearization techniques is extended and modified for application in time domain. Subsequently, an instantaneous expected value operator and the concept of instantaneous effective stiffness are proposed. The non-linear system is approximated at some instant during the step-response by a linear time-invariant mechanical system that utilizes the instantaneous effective stiffness concept. The oscillatory period of the non-linear step-response at that instant is then approximated by the natural period of the corresponding linear system. The proposed method is rigorously illustrated via two computational example cases (a near backlash and near pre-load non-linearities), and the necessary digital signal processing parameters for time domain analysis are investigated. Finally, the feasibility and applicability of the proposed method is demonstrated by estimating the softening and hardening trends in the time-varying oscillatory period of the measured response for two laboratory experiments that contain clearance elements and multi-staged torsional springs.

Keywords

Discontinuously non-linear systems, impact dynamics, digital signal processing, effective stiffness, impact dynamics, free vibration

Date received: 9 March 2016; accepted: 11 July 2016

Introduction

Most torque-transmission devices contain discontinuous non-linearities, such as clearances, multi-staged springs, pre-load elements, and stoppers[1–11]; prime examples of this family are vehicle powertrains and drivelines, which are composed of gears, spline shafts, synchronizers, and clutch dampers. This inherent set of non-linear features gives rise to undesirable vibro-impact phenomena, often known in the ground vehicle industry in terms of gear rattle[4,9] and vehicle driveline clunk[5–8] problems. Numerical and experimental studies concerning free vibration or step-response[5–8] clearly show regime-dependent (say double-sided or single-sided impact[9]) and time-varying oscillatory periods, as well as distinct asymptotic trends (hardening, softening, or linear).[4–11] In an effort to better understand previously observed results and assess such non-linear phenomena in measured or numerical motion signatures,[4–11] this paper will propose a new analysis tool. The chief goal is to estimate the trends in time-varying oscillatory periods of a non-linear torsional oscillator with a dual-staged spring and associated dry friction element. The method will be computationally verified and experimentally validated.

Analytical formulation of the problem

Consider a simple and yet representative time-invariant, non-linear torsional system described by a single degree of freedom (SDOF) model shown in Figure 1(a). The corresponding governing equation of motion is the following

$$J\ddot{\theta} + h\tanh\left(\eta\dot{\theta}\right) + \Phi(\theta) = T(t) \tag{1}$$

Acoustics and Dynamics Laboratory, Department of Mechanical and Aerospace Engineering, NSF Smart Vehicle Concepts Center, The Ohio State University, Columbus, OH, USA

Corresponding author:
Rajendra Singh, Acoustics and Dynamics Laboratory, Department of Mechanical and Aerospace Engineering, NSF Smart Vehicle Concepts Center, The Ohio State University, Columbus, OH 43210, USA.
Email: singh.3@osu.edu

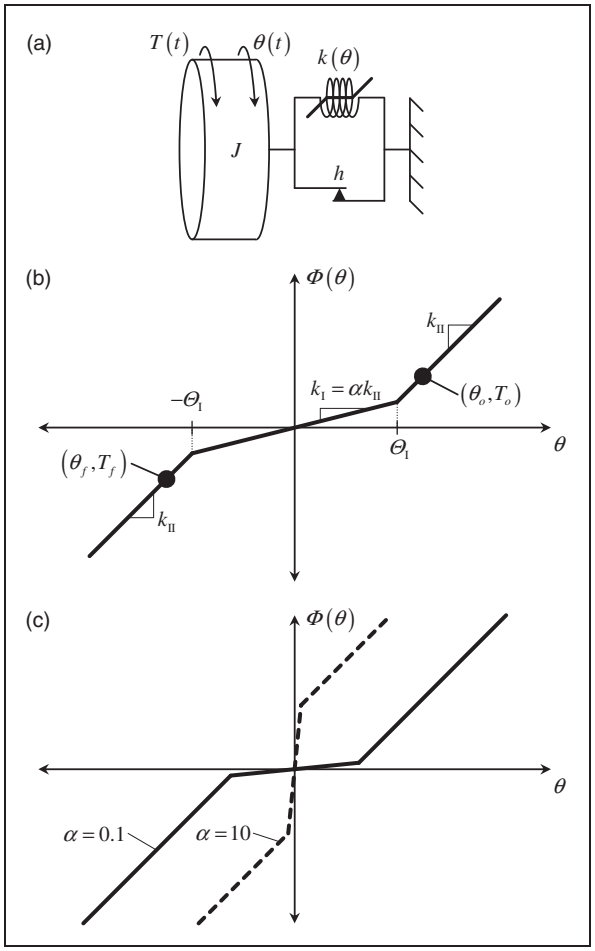

Figure 1. Conceptual illustration of the non-linear torsional system: (a) single degree of freedom model; (b) elastic torque $\Phi(\theta)$; and (c) examples of near backlash ($\alpha = 0.1$) and pre-load ($\alpha = 10$) non-linearities examined in this article. Here, θ is the angular displacement, J is the torsional inertia, h is a Coulomb friction element, $k(\theta)$ is a non-linear torsional stiffness element, and $T(t)$ is the external torque. Refer to the text or Appendix 1 for all symbols.

Here, θ is the angular displacement, J is torsional inertia, h is the Coulomb friction amplitude, η is an empirical regularizing factor,[12] $\Phi(\theta)$ is the torque transmitted through the stiffness element $k(\theta)$, and $T(t)$ is the external torque (see Appendix 1 for a full list of symbols). For the sake of simplicity, $k(\theta)$ is a symmetric dual-staged torsional spring as defined by the following equation where Ξ is the unit-step function, subscripts I and II denote stages, k_j is the stage-dependent torsional stiffness value, and Θ_j is an angular stage transition

$$k(\theta) = k_{\mathrm{I}} + (k_{\mathrm{II}} - k_{\mathrm{I}})\Xi(|\theta| - \Theta_{\mathrm{I}}) \tag{2}$$

Accordingly, $\Phi(\theta)$ is illustrated in Figure 1(b) and described by the following piece-wise linear equation where sgn is the triple-valued sign function

$$\Phi(\theta) = k_{\mathrm{I}}\theta + \mathrm{sgn}(\theta)(k_{\mathrm{II}} - k_{\mathrm{I}})(|\theta| - \Theta_{\mathrm{I}})\Xi(|\theta| - \Theta_{\mathrm{I}}) \tag{3}$$

The dynamic response within each stage only may be addressed by a linear sub-system with the corresponding natural periods

$$\tau_{nj} = 2\pi\left(J/k_j\right)^{0.5}, \quad j = \mathrm{I},\ \mathrm{II} \tag{4}$$

The stiffness of the first stage is scaled such that $k_{\mathrm{I}} = \alpha k_{\mathrm{II}}$ where $\alpha \geqslant 0$. For the case of backlash non-linearity with $\alpha = 0$, stage I is a clearance element and $\tau_{n\mathrm{I}} \to \infty$. However, when $\alpha \to \infty$, stage I is a pre-load feature and $\tau_{n\mathrm{I}} \to 0$; the limited case is $\alpha = 1$, where $k(\theta)$ is simply a linear spring. External torque $T(t)$ is a step applied at $t = 0$ and is such that the initial and final operating points ((θ_o, T_o) and (θ_f, T_f), respectively) lie on different stages, as shown in Figure 1(b). This ensures a comprehensive non-linear response with three distinct regimes and asymptotic trends of the time-varying oscillatory period, as seen in prior work.[4–8]

Specific objectives are as follows: (1) propose the instantaneous effective stiffness concept and utilize it to estimate the asymptotic trends of the time-varying oscillatory period; (2) propose the necessary digital signal processing parameters for related time domain analyses; and (3) validate the proposed method by estimating the asymptotic trends in the time-varying oscillatory period of two recent laboratory experiments.[8] The scope of this paper is limited to the time domain analysis of the step-response of time-invariant torsional systems. Additionally, it is assumed that damping can be approximated as Coulomb friction, and therefore, the oscillatory period may be approximated by the natural period of the first mode. This article extends the stochastic linearization techniques[13,14] proposed by Wallaschek[15] and Rook and Singh.[16]

Time-varying oscillatory period

The typical step-responses of the example case (Figure 1) is predicted for two illustrative cases, a near backlash non-linearity ($\alpha = 0.1$) and near pre-load non-linearity ($\alpha = 10$). The values of k_{II} and Θ_{I} are estimated from a production vehicle clutch damper.[8] Torsional inertia J is sized so that $\tau_{n\mathrm{II}} = 0.1$ s, which is within the range of the first torsional surge mode of a vehicle driveline.[4–9] The amplitudes of h, (θ_o, T_o), and (θ_f, T_f) are judiciously selected for each case so that the responses have similar durations though each is sufficiently long and exhibits the desired regimes. Angular motions are predicted through numerical integration1[17] of equation (1); several variable-step Runge–Kutta algorithms intended for low to high mathematically stiff systems are utilized,[17] but negligible differences between the results are found. Additionally, the maximum allowable time step for integration and the time resolution of resulting signals are set equal to approximately 78.1 μs, which corresponds to a sampling frequency of 12.8 kHz. The predicted angular

motions are shown in Figures 2 and 3; time and angular displacement are normalized by $\tau_{n\mathrm{II}}$ and Θ_{I}, respectively. Responses of Figures 2 and 3 exhibit three distinct regimes, similar to prior work[8]: (1) the double-sided impact regime (di) is characterized by θ crossing both $-\Theta_{\mathrm{I}}$ and Θ_{I}; (2) the single-sided impact regime (si) occurs when θ crosses $-\Theta_{\mathrm{I}}$ only; and (3) the no-impact regime (ni) is defined when θ does not cross any Θ_j.

The responses are further characterized by oscillatory period $\tau^{(j)}$ with corresponding time of occurrence $t^{(j)}$. Values $\tau^{(j)}$ and $t^{(j)}$ are defined as the elapsed and median times, respectively, between the j^{th} and $(j+2)^{\mathrm{th}}$ extrema (peak or valley) of a signal, as shown in Figures 2 and 3. A continuous time domain signal $\tau(t)$ is then calculated from a smoothened spline fit[17] of the discrete points $(t^{(j)}, \tau^{(j)})$ where $j = 1, 2, \ldots, P$ and P is the total number of oscillatory periods; calculated $\tau(t)$ is shown in Figure 4 for $\theta(t)$, $\dot{\theta}(t)$, and $\ddot{\theta}(t)$. It is observed that $\tau(t)$ calculations are similar across all angular motions and exhibit regime-dependent asymptotic trends, summarized in Table 1. These trends can be described as hardening ($\tau(t) \to 0$), softening ($\tau(t) \to \infty$), or linear ($\tau(t) \approx \tau_{nj}$) in nature. Next, a concept of instantaneous effective stiffness is proposed and later utilized to estimate $\tau(t)$.

Concept of instantaneous effective stiffness

Assume that over a small interval of time, with period τ_w centered at time $t = t'$, the following approximation[14–16] can be made $\{\Phi(\theta)\}|_{t=t'} \approx \{\hat{\Phi}(\theta)\}|_{t=t'}$; here, $\hat{\Phi}(\theta)|_{t=t'}$ is a linear time-invariant approximation of $\Phi(\theta)|_{t=t'}$. Like prior work,[15,16] $\hat{\Phi}(\theta)|_{t=t'}$ is defined by the following where $\hat{k}_m|_{t=t'}$ and $\hat{k}_a|_{t=t'}$ are mean and alternating stiffness components, respectively, and $\langle \theta, t' \rangle_t$ is the instantaneous expected value (windowed time average) of $\theta(t)$ over period τ_w centered at time $t = t'$

$$\left\{\hat{\Phi}(t)\right\}\Big|_{t=t'} = \left\{\hat{k}_m \langle \theta, t \rangle_t + \hat{k}_a [\theta(t) - \langle \theta, t \rangle_t]\right\}\Big|_{t=t'} \tag{5}$$

The proposed instantaneous expected value operator is defined by the following equation where $w_{\mathrm{shp}}(t - t')$ is a windowing function

$$\langle \theta, t' \rangle_t = \frac{\int_t \theta(t) w_{\mathrm{shp}}(t - t') \mathrm{d}t}{\int_t w_{\mathrm{shp}}(t - t') \mathrm{d}t} \tag{6}$$

The windowing function $w_{\mathrm{shp}}(t - t')$ has the following general form, chosen such that the instantaneous expected value operator can truly be localized

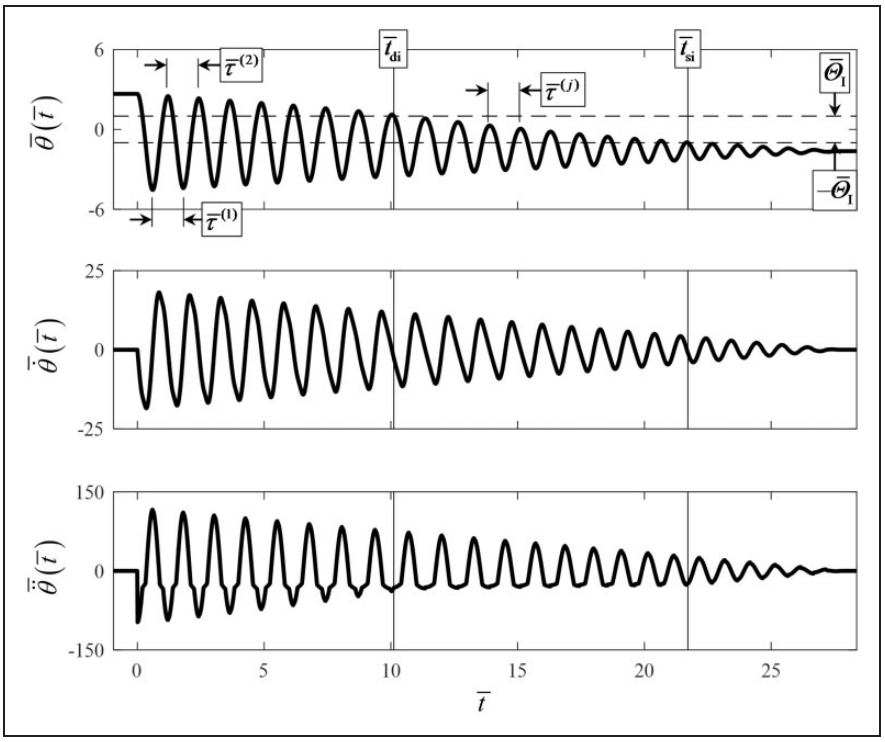

Figure 2. Predicted angular motions (normalized) for a backlash type non-linear system ($\alpha = 0.1$). Here, $\bar{\theta}$ is the angular displacement, $\dot{\bar{\theta}}$ is the angular velocity, $\ddot{\bar{\theta}}$ is the angular acceleration, $\bar{\tau}^{(j)}$ is oscillatory period j, $\bar{t}_{\mathrm{di}}$ is the time of transition from the double-sided to single-sided impact regimes, $\bar{t}_{\mathrm{si}}$ is the time of transition from the single-sided to no-impact regimes, and $\bar{\Theta}_{\mathrm{I}}$ is the angular transition from stage I to II. Key: (——)—angular motion; (– – –)—$\bar{\Theta}_{\mathrm{I}}$; and (|)—{$\bar{t}_{\mathrm{di}}$, $\bar{t}_{\mathrm{si}}$}.

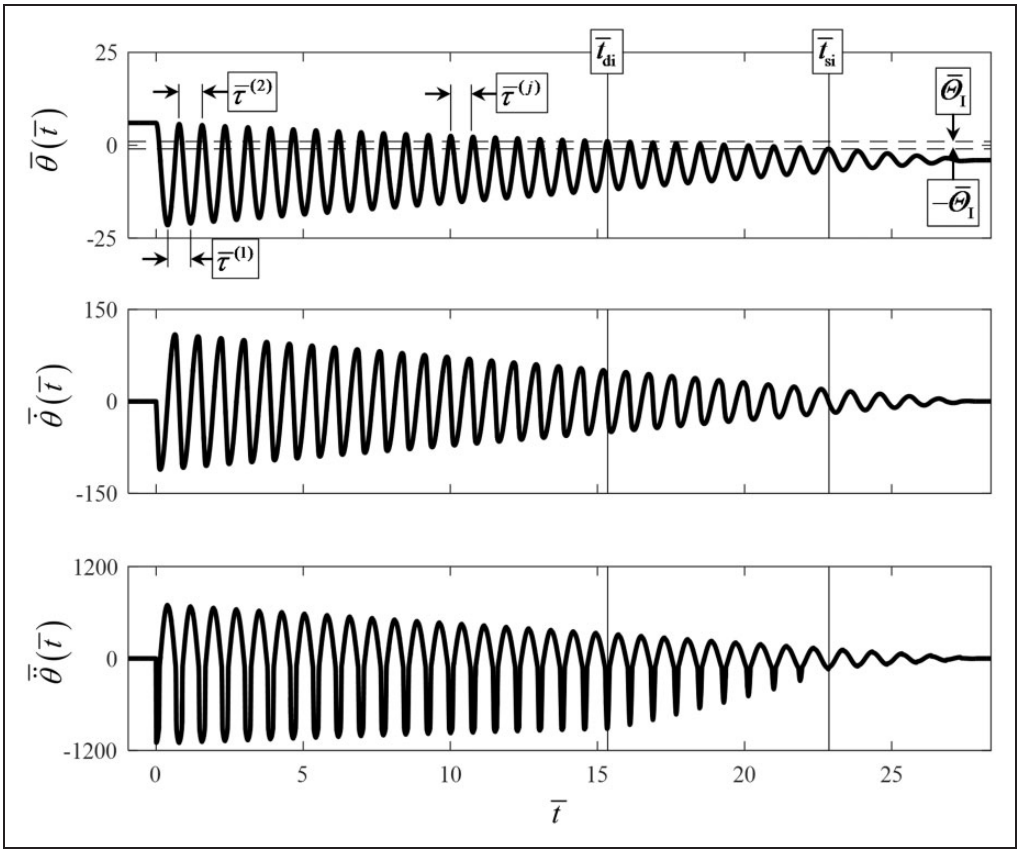

Figure 3. Predicted angular motions (normalized) for a pre-load type non-linear system ($\alpha = 10$). Here, $\bar{\theta}$ is the angular displacement, $\dot{\bar{\theta}}$ is the angular velocity, $\ddot{\bar{\theta}}$ is the angular acceleration, $\bar{\tau}^{(j)}$ is oscillatory period j, $\bar{t}_{di}$ is the time of transition from the double-sided to single-sided impact regimes, $\bar{t}_{si}$ is the time of transition from the single-sided to no-impact regimes, and $\bar{\Theta}_I$ is the angular transition from stage I to II. Key: (▬▬)—angular motion; (– – –)—$\bar{\Theta}_I$; and (|)—{$\bar{t}_{di}$, $\bar{t}_{si}$}.

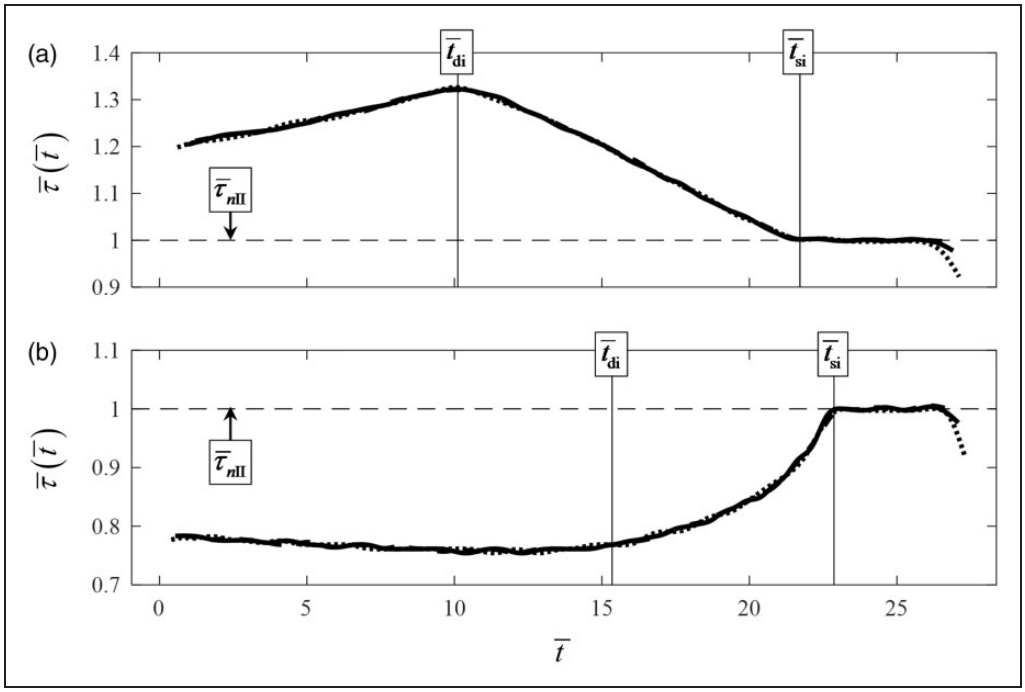

Figure 4. Calculated oscillatory period $\bar{\tau}(\bar{t})$ (normalized) for a torsional system with: (a) backlash type non-linearity ($\alpha = 0.1$) and (b) pre-load type non-linearity ($\alpha = 10$). Here, $\bar{\tau}_{nII}$ is the natural period of stage II, $\bar{t}_{di}$ is the time of transition from double-sided to single-sided impact regime, and $\bar{t}_{si}$ is the time of transition from the single-sided to no-impact regime. Key: (▬▬)—calculated from $\bar{\theta}(\bar{t})$; (▬ ▬)—calculated from $\dot{\bar{\theta}}(\bar{t})$; (▪▪▪▪▪)—calculated from $\ddot{\bar{\theta}}(\bar{t})$; (– – –)—$\bar{\tau}_{nII}$; and (|)—{$\bar{t}_{di}$, $\bar{t}_{si}$}.

Table 1. Regime-dependent asymptotic trends of $\bar{\tau}(\bar{t})$ for $\alpha = 0.1$ and $\alpha = 10$.

Regime	$\alpha = 0.1$	$\alpha = 10$
Double-sided impact (di)	Softening	Hardening
Single-sided impact (si)	Hardening	Softening
No-impact (ni)	Linear, $\bar{\tau}(\bar{t}) \approx \bar{\tau}_{nII}$	Linear, $\bar{\tau}(\bar{t}) \approx \bar{\tau}_{nII}$

in time

$$w_{\text{shp}}(t-t')\begin{cases} = 0 & t < t' - 0.5\tau_w \\ > 0 & t' - 0.5\tau_w \leqslant t \leqslant t' + 0.5\tau_w \\ = 0 & t > t' + 0.5\tau_w \end{cases} \tag{7}$$

To estimate $\hat{k}_m|_{t=t'}$ and $\hat{k}_a|_{t=t'}$, the following error is defined[15,16]

$$e|_{t=t'} = \{\Phi(\theta) - \hat{\Phi}(\theta)\}|_{t=t'} \tag{8}$$

Next, $\langle (e|_{t=t'})^2, t' \rangle_t$ is minimized with respect to $\hat{k}_m|_{t=t'}$ and $\hat{k}_a|_{t=t'}$ as follows

$$\frac{\partial \langle (e|_{t=t'})^2, t \rangle_t}{\partial \hat{k}_m\Big|_{t=t'}} = 0, \qquad \frac{\partial \langle (e|_{t=t'})^2, t \rangle_t}{\partial \hat{k}_a\Big|_{t=t'}} = 0 \tag{9}$$

Expanding equation (9), $\hat{k}_m|_{t=t'}$ and $\hat{k}_a|_{t=t'}$ are defined by

$$\hat{k}_m\Big|_{t=t'} = \frac{\langle \Phi, t' \rangle_t \langle \theta, t' \rangle_t}{\langle \theta, t' \rangle_t^2} \tag{10}$$

$$\hat{k}_a\Big|_{t=t'} = \frac{\langle \Phi\theta, t' \rangle_t - \langle \Phi, t' \rangle_t \langle \theta, t' \rangle_t}{\langle \theta^2, t' \rangle_t - \langle \theta, t' \rangle_t^2} \tag{11}$$

Following prior work,[15,16] instantaneous effective stiffness $\hat{k}|_{t=t'}$ is assumed to be equivalent to $\hat{k}_a|_{t=t'}$

$$\hat{k}\Big|_{t=t'} = \hat{k}_a\Big|_{t=t'} \tag{12}$$

However, $\hat{k}|_{t=t'}$ becomes undefined under static conditions; therefore, $t' \in [t_o + 0.5\tau_w,\ t_f - 0.5\tau_w]$ where t_o and t_f are the initial and final times of the dynamic response, respectively. Furthermore, t' and τ_w are restricted by sampling parameters and the duration of the dynamic response. Finally, a continuous time domain signal $\hat{k}(t)$ is calculated from a smoothened spline fit[17] of the discrete signal $\hat{k}|_{t=t'}$.

For the sake of illustration, $\bar{\hat{k}}(\bar{t})$ (normalized, $\bar{k}_{II} = 1$) is estimated over several w_{shp} and a range τ_w for a near backlash type non-linearity ($\alpha = 0.1$). The normalized window length $\bar{\tau}_w$ is limited to {0.5, 1, 2}, and windowing function w_{shp} is simply defined by the following (illustrated in Figure 5): (1) box-car w_{box}; (2) triangular w_{tri}; and (3) right-skewed saw-tooth w_{saw}. These three window shapes are chosen so that comparisons can be made between uniform and non-uniform weighting, and symmetric and asymmetric windows. The effect of window length $\bar{\tau}_w$ is shown in Figure 6 where w_{box} is utilized. It is clear that a smaller value of $\bar{\tau}_w$ produces a local estimation of $\bar{\hat{k}}(\bar{t})$; likewise, a larger value produces a global or smoothened estimation. Additionally, it is observed that the range of $\bar{\hat{k}}$ is bounded by physical stiffness elements $\bar{k}_{\text{I}}$ and $\bar{k}_{\text{II}}$. The effect of window shape is shown in Figure 7 where $\bar{\tau}_w = 1$. As before, $\bar{\hat{k}}(\bar{t})$ is bounded by $\bar{k}_{\text{I}}$ and $\bar{k}_{\text{II}}$ for all window shapes; however, each produces a unique result. Windows shapes which have a uniform weighting (w_{box}) give a smoothened estimation of $\bar{\hat{k}}$ compared to the windows that do not (w_{tri} and w_{saw}). It is also observed that estimations from asymmetric windows (w_{saw}) exhibit a time-shift effect when compared to the symmetric windows (w_{box} and w_{tri}).

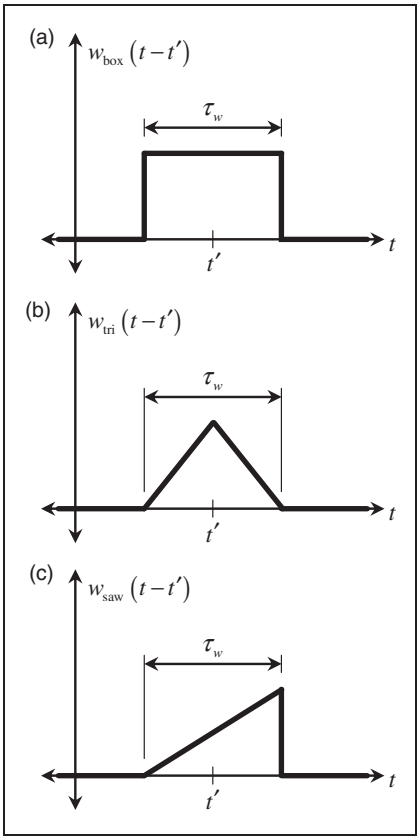

Figure 5. Uniform windowing functions w_{shp} used for estimations: (a) box-car, w_{box}; (b) triangular, w_{tri}; and (c) saw-tooth, w_{saw} where t' is an arbitrary time and τ_w is the window length.

It is important to note that $\hat{k}(t)$ is a mathematical concept (and not a physical spring element). Additionally, $\hat{k}|_{t=t'}$ is significantly different from $\langle k(\theta), t' \rangle_t$, which is the instantaneous expected value of $k(\theta)$ at $t = t'$ over τ_w. This is simply illustrated by the comparison of $\bar{\hat{k}}(\bar{t})$ to $\bar{k}_\mu(\bar{t})$ (a continuous time domain signal of $\langle k(\theta), t' \rangle_t$) for $\bar{\tau}_w = 1$ and w_{box}, as shown in Figure 8; the greatest absolute difference of $\bar{k}_\mu(\bar{t})$ with respect to $\bar{\hat{k}}(\bar{t})$ roughly 35%.

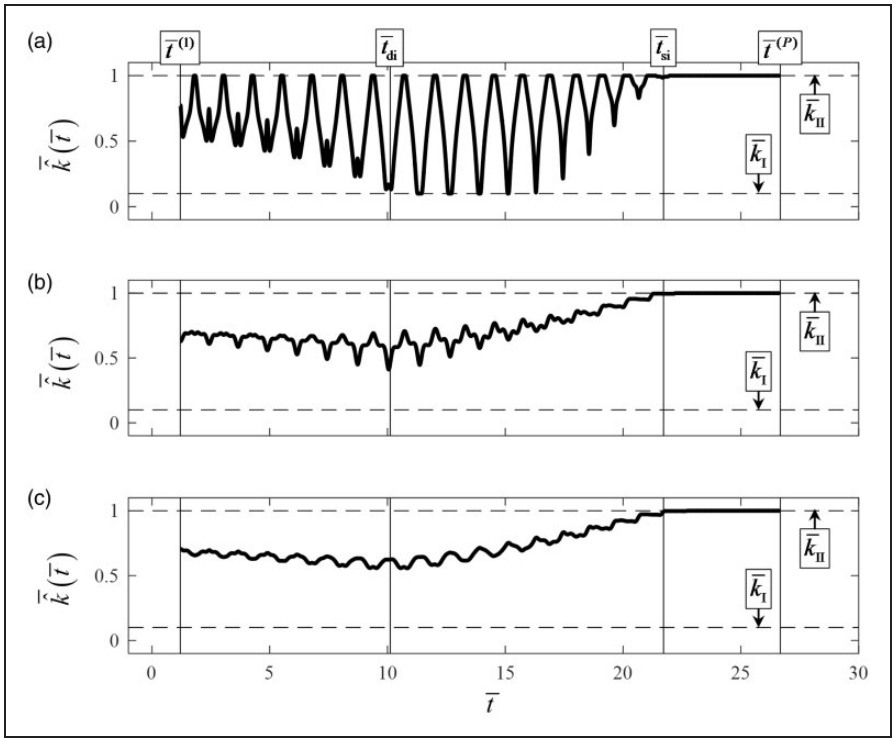

Figure 6. Instantaneous effective stiffness $\hat{\bar{k}}(\bar{t})$ (normalized) for a backlash type non-linear system ($\alpha = 0.1$) with windowing function w_{box} and uniform window lengths of: (a) $\bar{\tau}_w = 0.5$; (b) $\bar{\tau}_w = 1$; and (c) $\bar{\tau}_w = 2$. Here, $\bar{t}^{(1)}$ and $\bar{t}^{(P)}$ are the domain limits of $\bar{\tau}(\bar{t})$, $\bar{t}_{di}$ and $\bar{t}_{si}$ are regime transition times, and $\bar{k}_I$ and $\bar{k}_{II}$ are the torsional stiffness values for stages I and II, respectively. Key: (▬▬)—$\hat{\bar{k}}(\bar{t})$; (|)—$\{\bar{t}^{(1)},\ \bar{t}^{(P)},\ \bar{t}_{di},\ \bar{t}_{si}\}$; and (– – –)—$\{\bar{k}_{nI},\ \bar{k}_{nII}\}$.

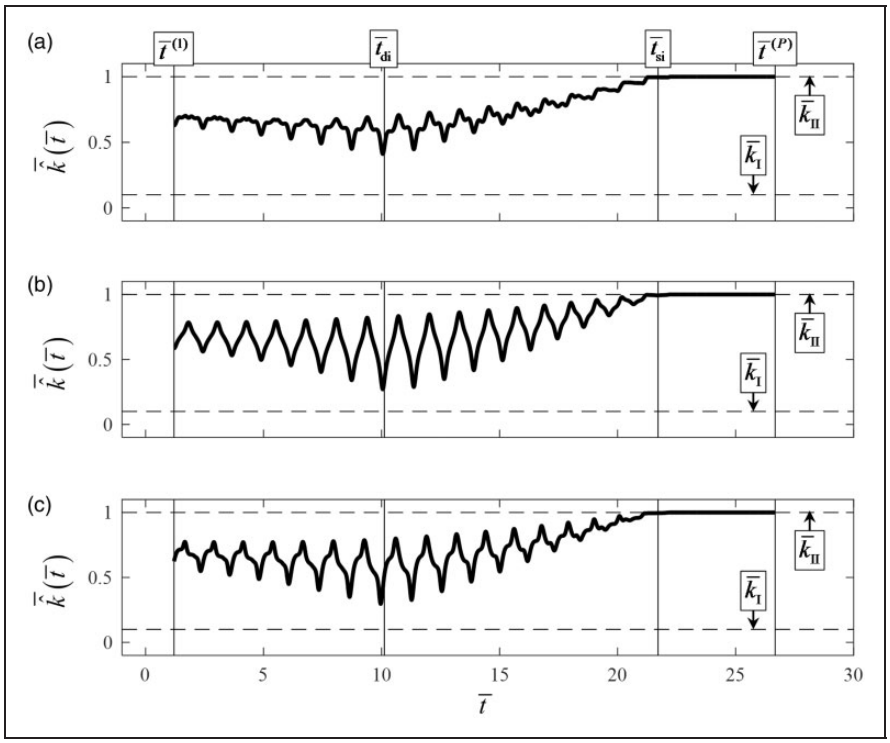

Figure 7. Instantaneous effective stiffness $\hat{\bar{k}}(\bar{t})$ (normalized) for a backlash type non-linear system ($\alpha = 0.1$) with uniform window length $\bar{\tau}_w = 1$ and the following windowing functions: (a) w_{box}; (b) w_{tri}; and (c) w_{saw}. Here, $\bar{t}^{(1)}$ and $\bar{t}^{(P)}$ are the domain limits of $\bar{\tau}(\bar{t})$, $\bar{t}_{di}$ and $\bar{t}_{si}$ are regime transition times, and $\bar{k}_I$ and $\bar{k}_{II}$ are the torsional stiffness values for stages I and II, respectively. Key: (▬▬)—$\hat{\bar{k}}(\bar{t})$; (|)—$\{\bar{t}^{(1)},\ \bar{t}^{(P)},\ \bar{t}_{di},\ \bar{t}_{si}\}$; and (– – –)—$\{\bar{k}_{nI},\ \bar{k}_{nII}\}$.

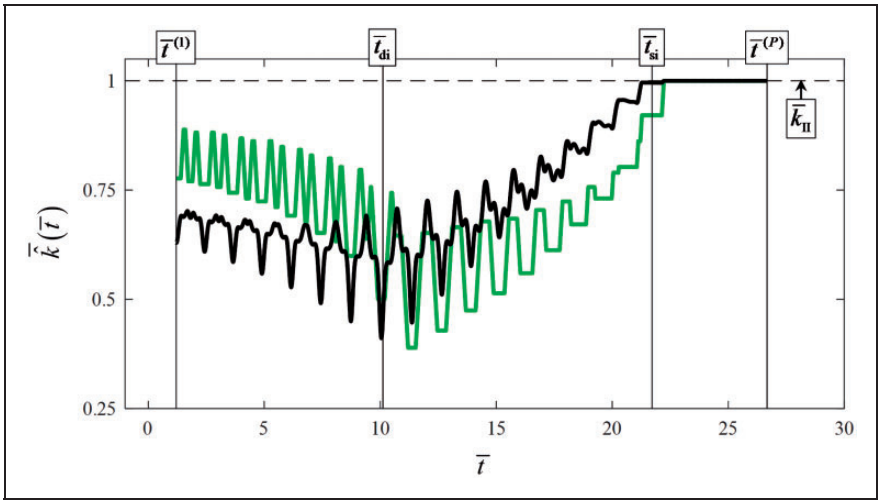

Figure 8. Instantaneous effective $\bar{\hat{k}}(\bar{t})$ and mean $\bar{k}_{\mu}(\bar{t})$ stiffness values (normalized) for a backlash type non-linear system ($\alpha = 0.1$) with uniform window length $\bar{\tau}_w = 1$, and windowing function w_{box}. Here, $\bar{t}^{(1)}$ and $\bar{t}^{(P)}$ are the domain limits of $\bar{\tau}(\bar{t})$, $\bar{t}_{di}$ and $\bar{t}_{si}$ are regime transition times, and $\bar{k}_{II}$ is the torsional stiffness of stage II. Key: (▬▬)—$\bar{\hat{k}}(\bar{t})$; (▬▬)—$\bar{k}_{\mu}(\bar{t})$; (|)—{$\bar{t}^{(1)}$, $\bar{t}^{(P)}$, $\bar{t}_{di}$, $\bar{t}_{si}$}; and (– – –)—$\bar{k}_{nII}$.

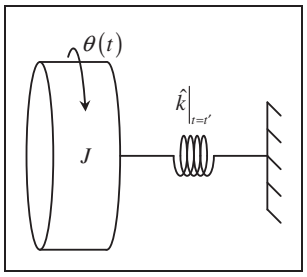

Figure 9. Effective undamped linear time-invariant system with instantaneous effective stiffness $\hat{k}|_{t=t'}$ at time $t = t'$ where θ is the angular displacement and J is the torsional inertia.

Equivalent linear system with instantaneous stiffness

At time $t = t'$, the SDOF non-linear system of Figure 1 may be approximated by an undamped time-invariant linear system (conceptually illustrated in Figure 9) consisting of torsional inertia J and torsional stiffness $\hat{k}|_{t=t'}$. The corresponding natural period (linear system) is

$$\hat{\tau}_n\big|_{t=t'} = 2\pi\left(J/\hat{k}\Big|_{t=t'}\right)^{0.5} \tag{13}$$

A continuous time domain signal $\hat{\tau}_n(t)$ is calculated from a smoothened spline fit[17] of $\hat{\tau}_n|_{t=t'}$; it is assumed that $\hat{\tau}(t) = \hat{\tau}_n(t)$ where $\hat{\tau}(t)$ is the estimated oscillatory period of the non-linear system. The normalized signal $\bar{\hat{\tau}}(\bar{t})$ is estimated for $\bar{\tau}_w \in [0.1,\ 6]$ across all w_{shp}; $\bar{\hat{\tau}}(\bar{t})$ for a near backlash type non-linearity ($\alpha = 0.1$) and $\bar{\tau}_w = 2$ is shown in Figure 10. For the sake of comparison to $\bar{\tau}(\bar{t})$ (which is calculated from $\bar{\theta}(\bar{t})$), the domain of $\bar{\hat{\tau}}(\bar{t})$ is limited to $\bar{t} \in [\bar{t}^{(1)},\ \bar{t}^{(P)}]$. The quantitative agreements between calculated $\bar{\tau}(\bar{t})$ and estimated $\bar{\hat{\tau}}(\bar{t})$ in the double-sided impact regime (di), single-sided impact regime (si), and the overall response (ov) are defined by metrics Π_{rr} where rr = {di, si, ov}

$$\Pi_{di} = \exp\left[-\int_{\bar{t}^{(1)}}^{\bar{t}_{di}} \left|\bar{\tau}(\bar{t}) - \bar{\hat{\tau}}(\bar{t})\right| d\bar{t}\right] \tag{14}$$

$$\Pi_{si} = \exp\left[-\int_{\bar{t}_{di}}^{\bar{t}_{si}} \left|\bar{\tau}(\bar{t}) - \bar{\hat{\tau}}(\bar{t})\right| d\bar{t}\right] \tag{15}$$

$$\Pi_{ov} = \exp\left[-\int_{\bar{t}^{(1)}}^{\bar{t}^{(P)}} \left|\bar{\tau}(\bar{t}) - \bar{\hat{\tau}}(\bar{t})\right| d\bar{t}\right] \tag{16}$$

If $\Pi_{rr} = 1$, then $\bar{\hat{\tau}}(\bar{t}) = \bar{\tau}(\bar{t})$ within the corresponding regime (deemed "best agreement"); otherwise, as $\Pi_{rr} \to 0$, then $|\bar{\tau}(\bar{t}) - \bar{\hat{\tau}}(\bar{t})| \to \infty$ (possibly the "worst agreement"). Metrics Π_{rr} for all w_{shp} and $\bar{\tau}_w$ are shown in Figure 11 (near backlash type non-linear, $\alpha = 0.1$) where $R[\bar{\tau}_{rr}]$ is the range of $\bar{\tau}(\bar{t})$ in the corresponding response regime. It is easily noted that all window shapes exhibit similar trends; there is increasing accuracy from $\bar{\tau}_w = 0.1$ to 1, followed by a leveling-off for roughly $1 \leqslant \bar{\tau}_w \leqslant 4$, and decreasing accuracy for $\bar{\tau}_w > 4$. However, the box-car window w_i has a slight loss of accuracy within $1 \leqslant \bar{\tau}_w \leqslant 2$. The maximum values of Π_{rr} and corresponding $\bar{\tau}_w$, say Π_{rr_best} and $\bar{\tau}_{w\_rr\_best}$, are listed in Tables 2 and 3, respectively. It is obvious that no single pairing of w_{shp} and $\bar{\tau}_w$ (within this limited set) achieves best accuracy for all response regimes and given range of α values, and that $\bar{\tau}_{w\_rr\_best}$ has a wide range across response regimes.

Nonetheless, one important observation is made: Best Π_{rr} is achieved when $R[\bar{\tau}_{rr}] \leqslant \bar{\tau}_w \leqslant 3R[\bar{\tau}_{rr}]$. However, a uniform τ_w might not satisfy this condition across all response regimes. Therefore, it stands to reason that a windowing function (w_{shp_adp}) that utilizes an adaptive window length ($\tau_w(t')$) could improve the accuracy. Therefore, the following new adaptive method is proposed: (1) An initial window length τ_{wo} is judiciously chosen; (2) Estimation of $\hat{k}|_{t=t'}$ is first estimated at time $t' = 0.5\tau_{wo}$ using the uniform

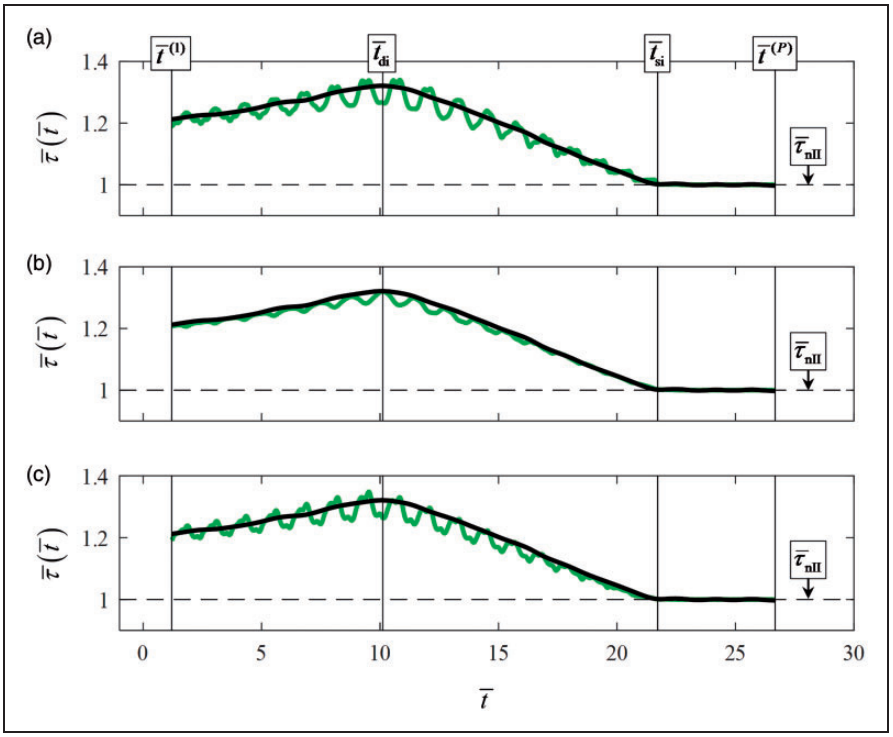

Figure 10. Calculated $\bar{\tau}(\bar{t})$ and estimated $\hat{\bar{\tau}}(\bar{t})$ oscillatory periods (normalized) for a backlash type non-linear system ($\alpha = 0.1$) with uniform window length $\bar{\tau}_w = 2$ and the following windowing functions: (a) w_{box}; (b) w_{tri}; and (c) w_{saw}. Here, $\bar{t}^{(1)}$ and $\bar{t}^{(P)}$ are the domain limits of $\bar{\tau}(\bar{t})$ and $\bar{t}_{di}$ and $\bar{t}_{si}$ are regime transition times. Key: (▬▬)—$\bar{\tau}(\bar{t})$; (▬▬)—$\hat{\bar{\tau}}(\bar{t})$; (|)—$\{\bar{t}^{(1)}, \bar{t}^{(P)}, \bar{t}_{di}, \bar{t}_{si}\}$; and (– – –)—$\bar{\tau}_{nII}$.

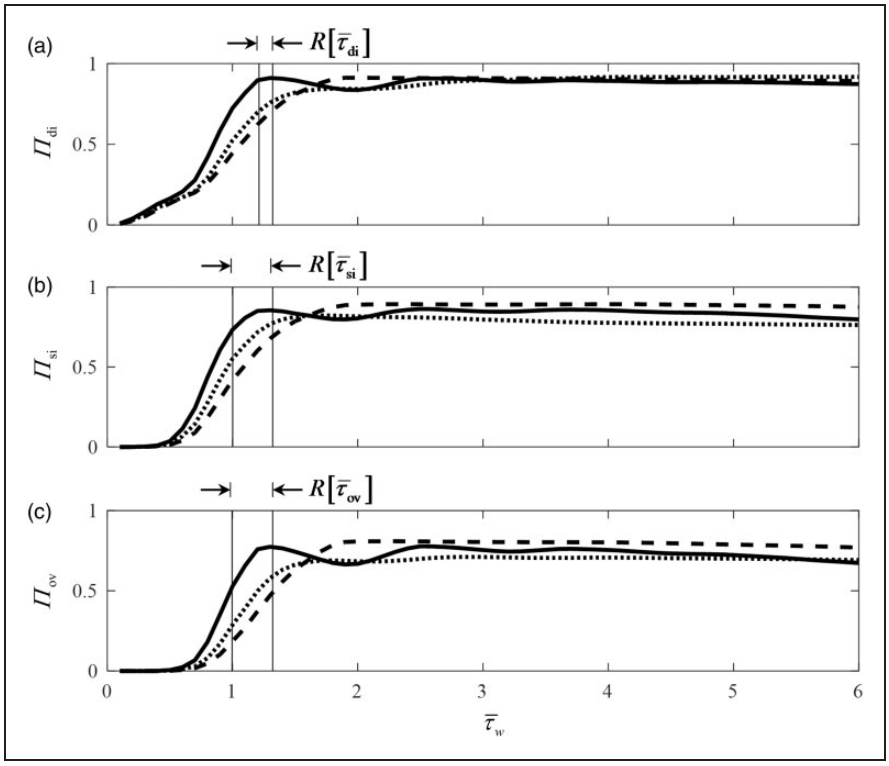

Figure 11. Regime-dependent metrics Π_{rr} for a backlash type non-linear system ($\alpha = 0.1$) with uniform window w_{shp_adp}. Here, $\bar{\tau}_w$ is the uniform window length (normalized), "di" is the double-sided impact regime, "si" is the single-sided impact regime, "ov" is the entire response, and $R[\bar{\tau}_{rr}]$ is the range of $\bar{\tau}(\bar{t})$ (observed) in regime "rr." Key: (▬▬)—w_{box}; (▬ ▬)—w_{tri}; (▪▪▪▪▪)—w_{saw}; and (|)—$R[\bar{\tau}_{rr}]$.

Table 2. Maximum values of estimation metrics Π_{rr_best} using uniform window w_{shp}.

Window shape (shp)	Π_{di_best}	Π_{si_best}	Π_{ov_best}
(a) $\alpha = 0.1$			
Box-car (box)	0.91	0.86	0.77
Triangular (tri)	0.91	0.89	0.81
Saw-tooth (saw)	0.92	0.82	0.71
(b) $\alpha = 10$			
Box-car (box)	0.84	0.90	0.74
Triangular (tri)	0.83	0.91	0.75
Saw-tooth (saw)	0.83	0.92	0.76

Table 3. Normalized window length $\bar{\tau}_{w\_rr\_best}$ necessary for Π_{rr_best} using uniform window w_{shp}.

Window shape (shp)	$\bar{\tau}_{w\_di\_best}$	$\bar{\tau}_{w\_si\_best}$	$\bar{\tau}_{w\_ov\_best}$
(a) $\alpha = 0.1$			
Box-car (box)	1.3	2.5	2.5
Triangular (tri)	2.0	4.1	2.2
Saw-tooth (saw)	5.4	1.7	2.9
(b) $\alpha = 10$			
Box-car (box)	1.7	3.1	1.7
Triangular (tri)	2.4	1.9	2.0
Saw-tooth (saw)	6.0	3.5	2.7

windowing function defined by equation (7) where $\tau_w = \tau_{wo}$; (3) For $t' > 0.5\tau_{wo}$, $\hat{k}|_{t=t'}$ is estimated using the following adaptive windowing function where $t'-$ is the time immediately prior to t', β is an arbitrary window length factor ($\beta > 0$), and $\tau_n|_{t=t'-}$ is the natural period of the time-invariant linear system at $t = t'^-$

$$w_{shp\_adp}(t-t')\begin{cases} = 0 & t < t' - 0.5\tau_w(t') \\ > 0 & t' - 0.5\tau_w(t') \leqslant t \leqslant t' + 0.5\tau_w(t') \\ = 0 & t > t' + 0.5\tau_w(t') \end{cases} \tag{17}$$

$$\tau_w(t') = 2\beta\pi\left(J/\hat{k}\Big|_{t=t'-}\right)^{0.5} = \beta\tau_n|_{t=t'-} \tag{18}$$

and (4) Estimated oscillatory period $\hat{\tau}|_{t=t'}$ (non-linear system) is then calculated from $\hat{k}|_{t=t'}$, and the related continuous time domain signal $\hat{\tau}(t)$ is calculated.[17]

For example, $\bar{\hat{\tau}}(\bar{t})$ is estimated using w_{shp_adp} over $0.1 \leqslant \beta \leqslant 6$, and the corresponding metrics Π_{rr} are shown in Figure 12 for a near backlash type non-linearity ($\alpha = 0.1$); here, $\tau_{wo} = 2t^{(1)}$. Accuracy increases from $\beta = 0.1$ to 1, then reaches its maximum within $1 \leqslant \beta \leqslant 4$, and decreases for $\beta > 4$. The β values for Π_{rr_best} (say β_{rr_best}) are given in Table 4. Similar to $\tau_{w\_rr\_best}$ for the uniform window, β_{rr_best} varies greatly across the response regimes; however, $1 \leqslant \beta_{ov\_best} \leqslant 3$ (roughly), which is consistent with the prior observation concerning τ_w. While β_{ov_best} is similar across α for w_{box_adp} and w_{tri_adp}, it has significant variation for w_{saw_shp}. A comparison of Π_{ov_best} for the

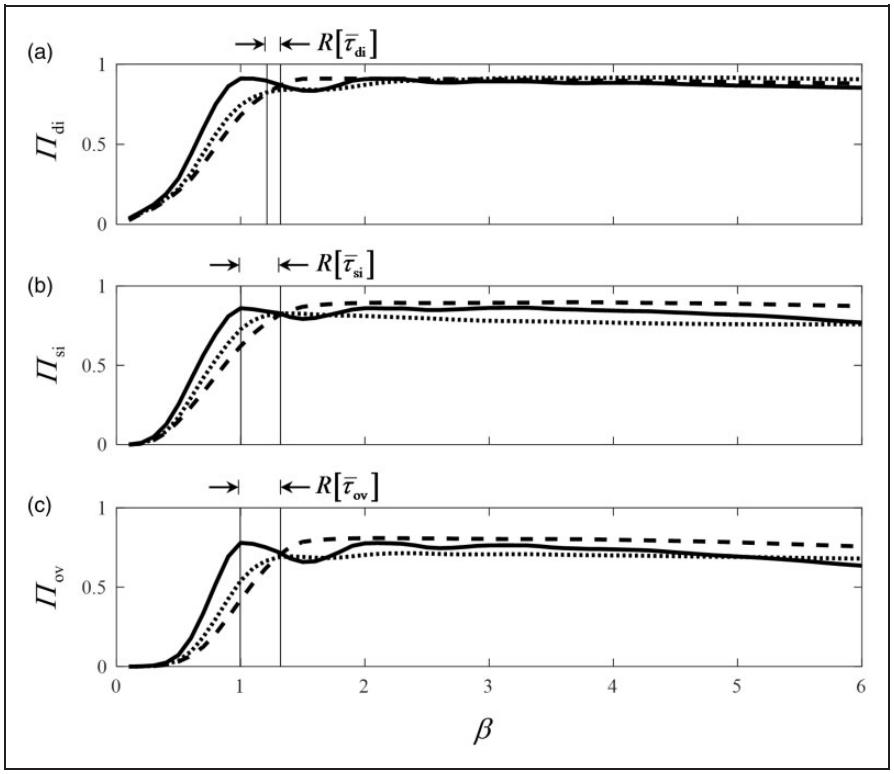

Figure 12. Regime-dependent metrics Π_{rr} for a backlash type non-linear system ($\alpha = 0.1$) with adaptive window w_{shp_adp}. Here, β is the window length factor, "di" is the double-sided impact regime, "si" is the single-sided impact regime, "ov" is the entire response, and $R[\bar{\tau}_{rr}]$ is the range of $\bar{\tau}(\bar{t})$ (observed) in regime "rr." Key: (▬▬)—w_{box_adp}; (▬ ▬)—w_{tri_adp}; (▪▪▪▪▪)—w_{saw_adp}; and (|)—$R[\bar{\tau}_{rr}]$.

Table 4. Window length coefficient β_{rr_best} necessary for Π_{rr_best} using adaptive window w_{shp_adp}.

Window shape (shp)	β_{di_best}	β_{si_best}	β_{ov_best}
(a) $\alpha = 0.1$			
Box-car (box)	1.0	3.3	1.0
Triangular (tri)	1.7	3.7	2.1
Saw-tooth (saw)	4.3	1.4	2.3
(b) $\alpha = 10$			
Box-car (box)	1.1	2.4	1.1
Triangular (tri)	2.8	2.0	2.0
Saw-tooth (saw)	4.6	3.5	3.5

Table 5. Summary of Π_{ov_best} for uniform and adaptive windows, $\Pi_{ov\_best}(w_{shp})$ and $\Pi_{ov\_best}(w_{shp\_adp})$, respectively.

Window shape (shp)	$\Pi_{ov\_best}(w_{shp})$	$\Pi_{ov\_best}(w_{shp\_adp})$
(a) $\alpha = 0.1$		
Box-car (box)	0.778	0.779
Triangular (tri)	0.809	0.810
Saw-tooth (saw)	0.711	0.714
(b) $\alpha = 10$		
Box-car (box)	0.736	0.742
Triangular (tri)	0.750	0.749
Saw-tooth (saw)	0.755	0.747

uniform and adaptive windows, ($\Pi_{ov\_best}(w_{shp})$ and $\Pi_{ov\_best}(w_{shp\_adp})$, respectively) is shown in Table 5; w_{shp_adp} improves overall accuracy for most but not all cases of α and window shape. Given these limited observations, it is recommended that w_{tri_adp} with $\beta \approx 2$ be utilized to achieve best possible accuracy in $\hat{\tau}(t)$ estimations. Although it is not addressed here, proper selection of τ_{wo} is also significant. Furthermore, $\tau_w(t')$, and thus β, are restricted by a choice of sampling parameters and the length of the dynamic response, similar to t' and τ_w.

In summary, the following observations are made regarding the window process: (1) Amplitude of $\hat{k}(t)$ is bounded by the stiffness values of the corresponding real spring for all windowing parameters; (2) Smaller window lengths produce a more temporally localized value, unlike larger lengths which give a more global value; (3) Uniformly and non-uniformly weighted window shapes (e.g. box-car w_{box} and triangular window w_{tri} shapes, respectively) of the same length can produce significantly different amplitudes; and (4) Asymmetric window shapes (e.g. saw-tooth w_{saw}) can produce a leading or lagging effect with respect to symmetric window shapes (e.g. box-car and triangular) of similar length.

Validation of estimation method using measurements from two laboratory experiments

To validate the proposed method, two laboratory experiments (X1 and X2), which can be approximated by the SDOF non-linear model illustrated in Figure 1, are considered next.[8,18] Experiment X1 is a controlled benchtop setup containing a single torsional clearance,[18] and X2 is a large-scale system containing a production vehicle clutch damper[8] (with four stages). The elastic function $\Phi(\theta)$ for each experiment is shown in Figure 13. External torque $T(t)$ is applied in a step-like manner with initial and final operating points lying on separate stages, as shown in Figure 13. The primary operating stages of X1 and X2 are II and III, respectively. Thus, the experiments are sized such that $\tau_{n\mathrm{II}} \approx 0.1$ s in X1 and $\tau_{n\mathrm{III}} \approx 0.1$ s; furthermore, normalized time for each system is scaled by these values.The time-varying oscillatory period $\tau(t)$ is calculated from measurements, as described in the section "Time-varying oscillatory period,", and shown in Figures 14 and 15; angular motions[8,18] are omitted for the sake of brevity. For experiment X1, only the double-sided impact regime (di) with a softening trend occurs; however, experiment X2 demonstrates all possible regimes and trends (although regime transition times are not labeled). This difference can be attributed to the following factors: (a) In X1, the final operating point $(\theta_f, \Phi_f) \approx (0, 0)$, whereas in X2, $(\theta_f, \Phi_f) \approx (\Theta_{\mathrm{I}}, > 0)$, which increases the likelihood that both double (di) and single-sided (si) impact regimes occur and (b) Energy dissipation has a large contribution to the response of X1 due to the

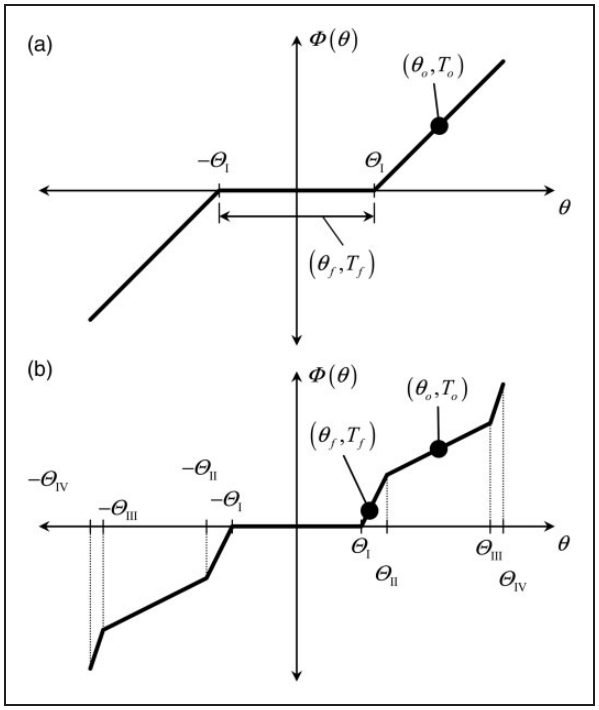

Figure 13. Illustration of multi-staged elastic torque curves $\Phi(\theta)$, and initial (θ_o, T_o) and final (θ_f, T_f) operating points for two experiments used to validate estimation methods: (a) experiment X1[18] and (b) experiment X2.[8] Here, θ is the angular displacement, T is external torque, Θ_j are angular stage transitions, and subscript {I, II,. . .} denote stages.

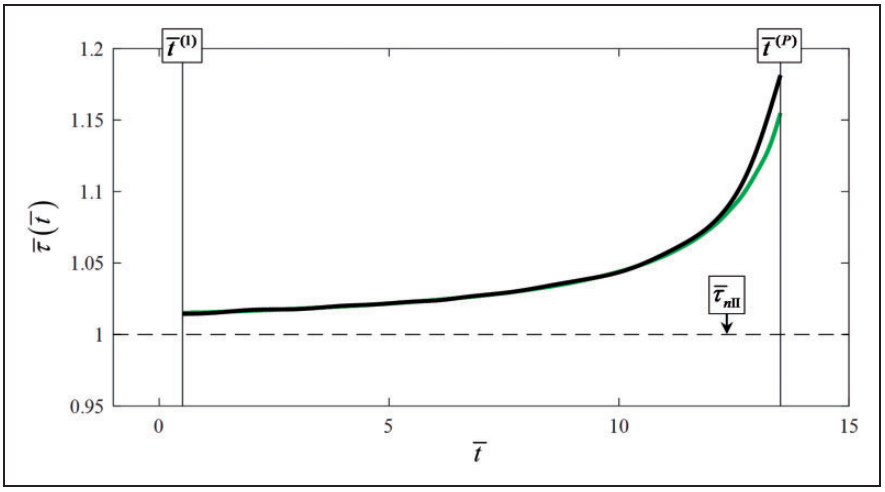

Figure 14. Calculated $\bar{\tau}(\bar{t})$ and estimated $\hat{\bar{\tau}}(\bar{t})$ oscillatory periods (normalized) for experiment X1 using adaptive windowing functionw_{tri_adp} with window length factor $\beta = 2$ and initial window length $\bar{\tau}_{wo} = 1$. Here, $\bar{t}^{(1)}$ and $\bar{t}^{(P)}$ are the domain limits of $\bar{\tau}(\bar{t})$. Key: (▬▬)—$\bar{\tau}(\bar{t})$; (▬▬)—$\hat{\bar{\tau}}(\bar{t})$; (|)—$\{\bar{t}^{(1)},\ \bar{t}^{(P)}\}$; and (– – –)—$\bar{\tau}_{nIII}$.

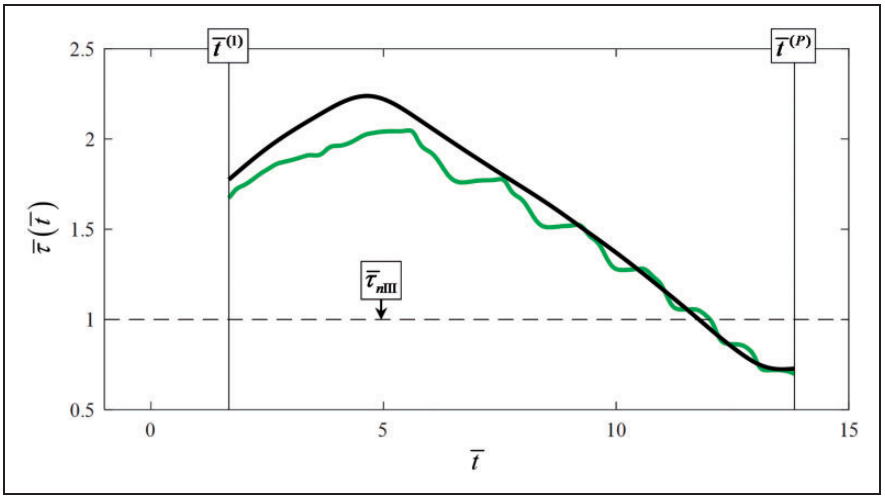

Figure 15. Calculated $\bar{\tau}(\bar{t})$ and estimated $\hat{\bar{\tau}}(\bar{t})$ oscillatory periods (normalized) for experiment X2 using adaptive windowing functionw_{tri_adp} with window length factor $\beta = 2$ and initial window length $\bar{\tau}_{wo} = 1$. Here, $\bar{t}^{(1)}$ and $\bar{t}^{(P)}$ are the domain limits of $\bar{\tau}(\bar{t})$. Key: (▬▬)—$\bar{\tau}(\bar{t})$; (▬▬)—$\hat{\bar{\tau}}(\bar{t})$; (|)—$\{\bar{t}^{(1)},\ \bar{t}^{(P)}\}$; and (– – –)—$\bar{\tau}_{nII}$.

presence of a backlash non-linearity ($k_I = 0$), unlike X2 for which k_I is a very soft spring.

Following the suggestions from Section 5, $\hat{\tau}(t)$ signals for both X1 and X2 are estimated using w_{tri_adp} with $\beta = 2$; an initial guess of $\bar{\tau}_{wo} = 1$ is selected. Quantitative comparisons between $\bar{\tau}(\bar{t})$ (observed) and $\hat{\bar{\tau}}(\bar{t})$ (estimated) are shown in Figures 14 and 15 for experiments X1 and X2, respectively. In particular, the signal $\hat{\bar{\tau}}(\bar{t})$ correctly exhibits the hardening and softening nature observed in each experiment though it lacks complete agreement with $\bar{\tau}(\bar{t})$. Several factors could contribute to this difference. First, the suggested windowing parameters and algorithm (developed from simplified example cases) may not be optimal for these real experiments. Furthermore, the corresponding non-linear models of these experiments may require additional degrees of freedom and the corresponding features would need a higher level of characterization. Finally, if significant viscous damping is present with a relatively low stiffness, then the oscillatory period cannot be accurately estimated by an effective natural period. Instead, an effective damped natural period would need to be considered.

Conclusion

The main contribution of the paper is the development of a new analysis tool that estimates the trends in time-varying oscillatory periods in the step-response of a torsional system containing a multi-staged spring. Development of the method begins with the formulation of a new concept of instantaneous effective stiffness. Although it is strictly mathematical in nature (and not a physical element), its amplitude is limited by the stiffness values of the corresponding real spring. The related computations

employ windowing functions, and thus a range of window shapes and lengths are investigated. Next, the instantaneous effective stiffness is used to approximate the real non-linear system (at some instant during its step-response) as an undamped time-invariant linear oscillator. Here, it is assumed that the damping in the real system is relatively low such that its oscillatory period at that time can be approximated by the natural period of the linear oscillator. The method is then applied to numerical example cases and a set of windowing parameters, which include window shape and an adaptive length algorithm, are suggested from the results. Finally, the proposed method is validated by correctly estimating the asymptotic trends (such as hardening or softening) observed in the time-varying oscillatory periods of two recently proposed experiments by the authors.[8,17] Although measured (or numerically simulated) responses must be known to calculate the instantaneous effective stiffness, the utility of this concept demonstrates its relationship to the non-linear response. Specifically, this time domain concept correctly identifies hardening and softening trends, which have been historically discussed in the context of harmonic excitation.[9,11,16] The method of this article should serve as an important diagnostic tool for the system identification of an unknown device. Assuming that angular displacement and torque can be measured for a step-response, the proposed method should provide value insight for the characterization of non-linear features (say using a SDOF approximation), as well as amplitude dependence.[19] In cases of relatively high viscous damping, the method could be applied to only the first few cycles of oscillations. Overall, the proposed method should improve the efficiency and accuracy of the model building process for mechanical devices with clearance non-linearities.[2,19]

Acknowledgement

The authors acknowledge Eaton Corporation (Clutch Division) for supporting this research. We would like to thank Luiz Pereira and Brian Franke for their assistance with experimental studies. Further, we acknowledge the member organizations of the Smart Vehicle Concepts Center (www.SmartVehicleCenter.org) and the National Science Foundation.

Declaration of Conflicting Interests

The author(s) declared no potential conflicts of interest with respect to the research, authorship, and/or publication of this article.

Funding

The author(s) received no financial support for the research, authorship, and/or publication of this article.

References

1. Den Hartog JP. *Mechanical vibrations*. 4th ed. New York: McGraw-Hill, 1956.
2. Ibrahim RA. Recent advances in nonlinear passive vibration isolators. *J Sound Vib* 2008; 314: 371–452. DOI: 10.1016/j.jsv.2008.01.014.
3. Shaver F. *Manual transmission clutch systems*. Warrendale, Pennsylvania, USA: SAE, 1997.
4. Couderc P, Callenaere J, Der Hagopian J, et al. Vehicle driveline dynamic behavior: experimentation and simulation. *J Sound Vib* 1998; 218: 133–157. DOI: 10.1006/jsvi.1998.1808.
5. Biermann JW and Hagerodt B. Investigation of the clonk phenomenon in vehicle transmissions – measurement, modelling, and simulation. *Proc IMechE, Part K: J Multi-body Dynamics* 1999; 213: 53–60. DOI: 10.1243/1464419991544054.
6. Menday MT, Rahnejat H and Ebrahimi M. Clonk: an onomatopoeic response in torsional impact of automotive drivelines. *Proc IMechE, Part D: J Automobile Engineering* 1999; 213: 349–357. DOI: 10.1243/0954407991526919.
7. Crowther AR, Singh R, Zhang N, et al. Impulsive response of an automatic transmission system with multiple clearances: formulation, simulation, and experiment. *J Sound Vib* 2007; 306: 444–466.
8. Krak MD, Dreyer JT and Singh R. Development of a non-linear clutch damper experiment exhibiting transient dynamics. *SAE Int J Passeng Cars Mech Syst* 2015; 8: 754–761.
9. Comparin RJ and Singh R. An analytical study of automotive neutral gear rattle. *ASME J Mech Des* 1990; 112: 237–245.
10. Babitsky VI and Krupenin VL. *Vibration of strongly nonlinear discontinuous systems*. Berlin: Springer, 2001.
11. Dubowsky S. Dynamic analysis of mechanical systems with clearances part 2: dynamic response. *J Eng Ind* 1971; 93: 305–309.
12. Kim TC, Rook TE and Singh R. Effect of smoothening function on the frequency response of an oscillator with clearance non-linearity. *J Sound Vib* 2003; 263: 665–678.
13. Crandall SH. A half-century of stochastic equivalent linearization. *Struct Contr Health Monit* 2006; 13: 27–40.
14. Iwan WD and Mason AB. Equivalent linearization for systems subjected to non-stationary random excitation. *Int J Nonlinear Mech* 1980; 15: 71–82.
15. Wallaschek J. Dynamics of non-linear automobile shock-absorbers. *Int J Nonlinear Mech* 1990; 25: 299–308. DOI: 10.1016/0020-7462(90)90059-I.
16. Rook TE and Singh R. Dynamic analysis of a reverseidler gear pair with concurrent clearances. *J Sound Vib* 1995; 182: 303–322. DOI: 10.1006/jsvi.1994.0198.
17. MathWorks. MATLAB, http://www.mathworks.com/products/matlab/ (accessed January 2016).
18. Krak MD and Singh R. Practical and controlled laboratory vibration experiments that demonstrate the impulsive response of multi-staged clutch dampers. In: *INTER-NOISE 2015*, San Francisco, CA, 9–12 August 2015, paper no. 58.
19. Kerschen G, Worden K, Vakakis AF, et al. Past, present and future of nonlinear system identification in structural dynamics. *Mech Syst Signal Process* 2006; 20: 505–592. DOI: 10.1016/j.ymssp.2005.04.008.

Appendix I

Notation

e	error
h	Coulomb friction amplitude
J	torsional inertia
k	torsional stiffness
N	total number of stiffness stages
t	time
T	external torque
w	windowing function
α	stiffness stage ratio
β	window length coefficient
Γ	total torque transmission
η	regularizing factor for Coulomb friction
$\theta, \dot{\theta}, \ddot{\theta}$	angular displacement, velocity, and acceleration
Θ	stage transition (angular)
Π	estimation metric
τ	period of oscillation
Φ	elastic torque
Ξ	unit-step function
Ψ	dissipative torque

Subscripts

a	alternating coefficient
adp	adaptive window
best	"best"
box	box-car
di	double-sided impact
f	final point
m	mean coefficient
n	natural
ni	no-impact
o	initial point
ov	overall response
rr	upright
saw	saw-tooth
shp	shape
si	single-sided impact
t	instantaneous (time dependent)
tri	triangular
w	windowing function
I, II, ...	stage index

Superscripts

(i)	oscillatory period number ($i = 1, 2, \ldots, P$)
$\hat{}$	effective